A spatial representation of information underlies probabilistic computation in cells

Matt Thomson[1*], Zitong Jerry Wang[2*]

[1]Division of Biology and Biological Engineering, Caltech, Pasadena & 91125, USA.

[2]Center for Interdisciplinary Studies, School of Science, Westlake University, Hangzhou & 310024, P. R. China.

[*]Corresponding authors. Email: mthomson@caltech.edu, jerry@westlake.edu.cn

Seeking a signal source in unstructured environments is a fundamental challenge in robotics. Similarly, cells in tissues track signal sources using noisy, fragmented molecular gradients, shaped by fluid flow and extracellular matrix interactions. However, the precise algorithm cells use for source seeking is unknown. We show that cells can perform source seeking using a biophysical implementation of a computational algorithm called Bayes filtering. Specifically, the spatial distribution of molecules within the cell encodes a probability distribution over source location, and intracellular transport processes update this distribution. Live-cell imaging and spatial proteomics reveal that receptor dynamics in vivo matches the evolution of belief distributions under Bayes filtering. Unlike standard Bayes filtering, the cellular implementation adapts to fluctuating measurement noise without explicitly estimating noise statistics. When translated to traditional robotics algorithms, this cell-inspired adaptation enables robust navigation without continuously estimating signal statistics. Our results show that cells can leverage spatial organization to implement probabilistic algorithms, bridging cellular behavior and engineered systems.

Source seeking is classic robotics task, where a robot must localize toward the source of a signal.

For example, aerial drones are used to find the source of gas leaks (*1*), or underwater robots are deployed to identify chemical spills. In practice, uncertain environmental conditions like turbulent flow can break continuous signal gradients into discontinuous patches (*2*), where deterministic algorithms like gradient descent risks trapping robots in local signal patches (Figure 1A).

Probabilistic methods for source seeking are often more effective than deterministic algorithms in unstructured environments, but are known to be computationally-intensive (*3*). In these algorithms, the agent maintains a probability distribution $\text{bel}(x_t)$ over all possible source positions $x_t \in \Omega$ and iteratively updates this belief using sensor measurements Z_t (Figure 1A). The core update rule underlying most such algorithm is given by the Bayes filter (*3*):

$$\text{bel}\,(x_t) = \eta\; p\,(Z_t \mid x_t) \int_{\Omega} p\,(x_t \mid x_{t-1})\,\text{bel}\,(x_{t-1})\,dx_{t-1}. \tag{1}$$

which yields the minimum mean squared error estimate of the true target position assuming accurate models. The algorithm consists of three steps: a prediction step to account for uncertainty in movement, where the prior belief $\text{bel}\,(x_{t-1})$ is convolved with the motion model $p(x_t|x_{t-1})$, followed by an update step to incorporate new sensor reading, where the belief is reweighted by the measurement likelihood $p(Z_t|x_t)$. Lastly, a normalization term η ensures belief sums to one. While effective, this iterative process is resource-intensive, requiring integration over the state space at each step and memory to store a full belief distribution over all candidate spatial locations.

Cells can efficiently localize to ligand sources in complex tissue environments, overcoming local signal peaks despite relying on noisy chemical hardware and operating under tight resource budgets. In tissues, extracellular matrix (ECM) binding and interstitial fluid flow break ligand gradients into irregular, fragmented patches (*4–8*). For example, CCL21, a chemokine secreted by lymphatic endothelial cells to guide cells toward lymphatic vessels, is transported by fluid flow and captured by a non-uniform ECM network. Quantitative imaging of mouse ear dermis shows that CCL21 forms a stable, reticulated pattern with local concentration peaks (*7*). CCL21 gradients appear smooth when averaged over tissue-scale regions, but vector field of local gradients, computed at the scale of individual cells (Figure 1B), reveal highly conflicting cues where local gradients often fail to align with the true source direction. These patchy gradients are stable over time due to strong ECM binding (*9*), having been observed for other morphogens and chemokines in vivo (*10–12*). This navigation problem is analogous to non-convex optimization, where naive

gradient descent only achieves local optima. Despite these challenges, live-cell imaging shows that cells can efficiently reach ligand sources (*7*), suggesting they use strategies that go beyond simple gradient-following.

Recent observations suggest dynamic spatial rearrangement of surface receptors may be important for source seeking tasks such as tracking and navigation. In neuronal growth cones, receptors such as Robo1 and PlxnA1 reorganize according to local ligand distributions, and inhibiting their rearrangement impairs directional guidance (*13,14*). In budding yeast, pheromone receptors dynamically rearrange to track the pheromone source during mating. In mesenchymal stem cells, blocking CCR2 receptor redistribution, without changing its overall expression, severely disrupts targeted migration to injured muscle tissues (*15*). These observations suggest that receptor dynamics, and not just expression, can be pivotal for robust source seeking.

In this work, we show that dynamic receptor rearrangement can function as a biophysical implementation of the Bayes filtering algorithm optimized for source seeking in complex environments. The spatial distribution of receptors encodes a probability distribution over source location and intracellular transport processes can update this distribution, thereby implementing key steps of the algorithm. Live-cell imaging and spatial proteomics data show that the Bayes filtering update rule accurately predicts the spatiotemporal dynamics of cell-surface receptors during source seeking. Unlike conventional Bayes filtering, the cellular implementation adapts to fluctuating measurement noise without explicitly estimating noise statistics. We show that translating this cell-inspired adaptation back into traditional robotics algorithms enables robust source seeking without the need to continuously estimate signal statistics. Our results illustrate how cells leverage spatial organization to implement complex, probabilistic algorithms.

Receptor redistribution can implement Bayes filtering

We show that cells can implement an exact Bayes filter using known intracellular transport processes. To make this mapping concrete, we first construct a minimal Bayesian filter that is memory-efficient and computationally tractable (Figure 1B). We define the hidden state as the source direction $\theta_t \in [-\pi, \pi)$ relative to the agent's location. This choice, rather than using the full coordinate space, minimizes memory demands. We discretize this variable into N possible directions, $\theta_t = 2\pi i/N$

for $i = 1, \ldots, N$, with belief $P_i^t = P(\theta_t = 2\pi i/N)$ and input signal $C_t \in \mathbb{Z}^N$ representing ligand counts across membrane sectors. To simplify the prediction step, we use a Gaussian motion model to capture stochastic shifts in the source direction given cell movement:

$$\theta_t|\theta_{t-1} \sim \mathcal{N}(\theta_{t-1}, \sigma^2). \tag{2}$$

Assuming small variance reduces the integral in Equation (1) to a weighted sum:

$$\sigma(P_{i-1}^{t-1} + P_{i+1}^{t-1}) + (1 - 2\sigma)P_i^{t-1}.$$

Next, we assume the measurement likelihood depends only on the ligand level in the source direction being conditioned on. We obtain a linear approximation of the likelihood model by fitting to signals sampled from interstitial gradients (*16*):

$$p(C_t|\theta_t = 2\pi i/N) \approx \alpha(1 + \beta C_i^t), \tag{3}$$

where $C_i^t = C_t(\theta_t = 2\pi i/N)$. This model expresses how likely a ligand profile is, given the true source location. Note that β is small but positive, indicating that higher ligand counts only marginally increase the likelihood of a source, reflecting the patchiness of the signals. Substituting the motion model and measurement likelihood into Equation (1) yields a minimal Bayes filter for source seeking.:

$$P_i^t = \eta(1 + \beta C_i^t)[\sigma(P_{i-1}^{t-1} + P_{i+1}^{t-1}) + (1 - 2\sigma)P_i^{t-1}], \tag{4}$$

where η absorbed the constant factor from Equation (3) and represents the normalization step of the algorithm.

Receptor redistribution provides an exact biophysical implementation of the Bayesian filtering algorithm, where the spatial distribution of receptors encodes the belief distribution, and intracellular transport processes update it over time (Figure 1C). We show in the SI (*16*) that the minimal Bayes filter update of Equation (4) is mathematically equivalent to a standard partial differential equation (PDE) model describing receptor transport:

$$\frac{\partial R(x,t)}{\partial t} = D_m \nabla^2_{\text{memb}} R - k_{\text{off}} R + hAR_{\text{cyto}}. \tag{5}$$

Here $R(x,t)$ denotes the receptor concentration along the cell surface at location x and time t. This receptor profile represents the posterior belief P in the Bayes filter, as the rate of change of

receptor across the cell surface $\partial R/\partial t$ is equivalent to the Bayes belief update (Equation 4). Each step of this filtering algorithm maps to a term in the PDE. The motion model (Equation 2) maps to lateral receptor diffusion, represented by the Laplacian $\nabla^2_{\text{memb}} R$, where membrane diffusivity D_m corresponds to the motion model variance σ^2. The measurement likelihood (Equation 3) maps to exocytosis from a cytosolic pool at rate hAR_{cyto}, polarized toward regions with high receptor activity creating a positive feedback. Here, likelihood model parameter β corresponds to rate constant h. Lastly, normalization (η) maps to receptor endocytosis with rate k_{off} (Figure 1C). In this way, filter updates of the belief correspond to receptor redistribution on the cell, and cells moving in the direction of maximal receptor activity approximately follows the maximum a posteriori estimate of the true source direction.

Polarized exocytosis of receptors for guidance cue (*14,17,18*), pheromones (*19*), chemokines (*15, 20*), and growth factors (*21, 22*) involve multiple intermediate processes, which could vary between receptors (*23*). For example, activation of DCC receptors by chemoattractant Netrin-1 lead to ligand-dependent clustering of DCC/Sytx1 complexes in activated membrane domains. Here, the formation of a SNARE complex between Sytx1 and TI-VAMP proteins occurs, thereby promoting exocytosis of DCC-containing vesicles at DCC-activated domains (*24*). For nerve growth factor (NGF), local activation of NGF receptors in growth cones induces asymmetric vesicle trafficking and targeted insertion of additional NGF receptors into the membrane near the site of stimulation via VAMP2-dependent exocytosis (*21*). Note some receptors may not redistribute in the manner described above (*25, 26*), since cells may implement Bayes filtering through membrane-bound effectors downstream of receptor activation rather than through receptor movement (see Discussion).

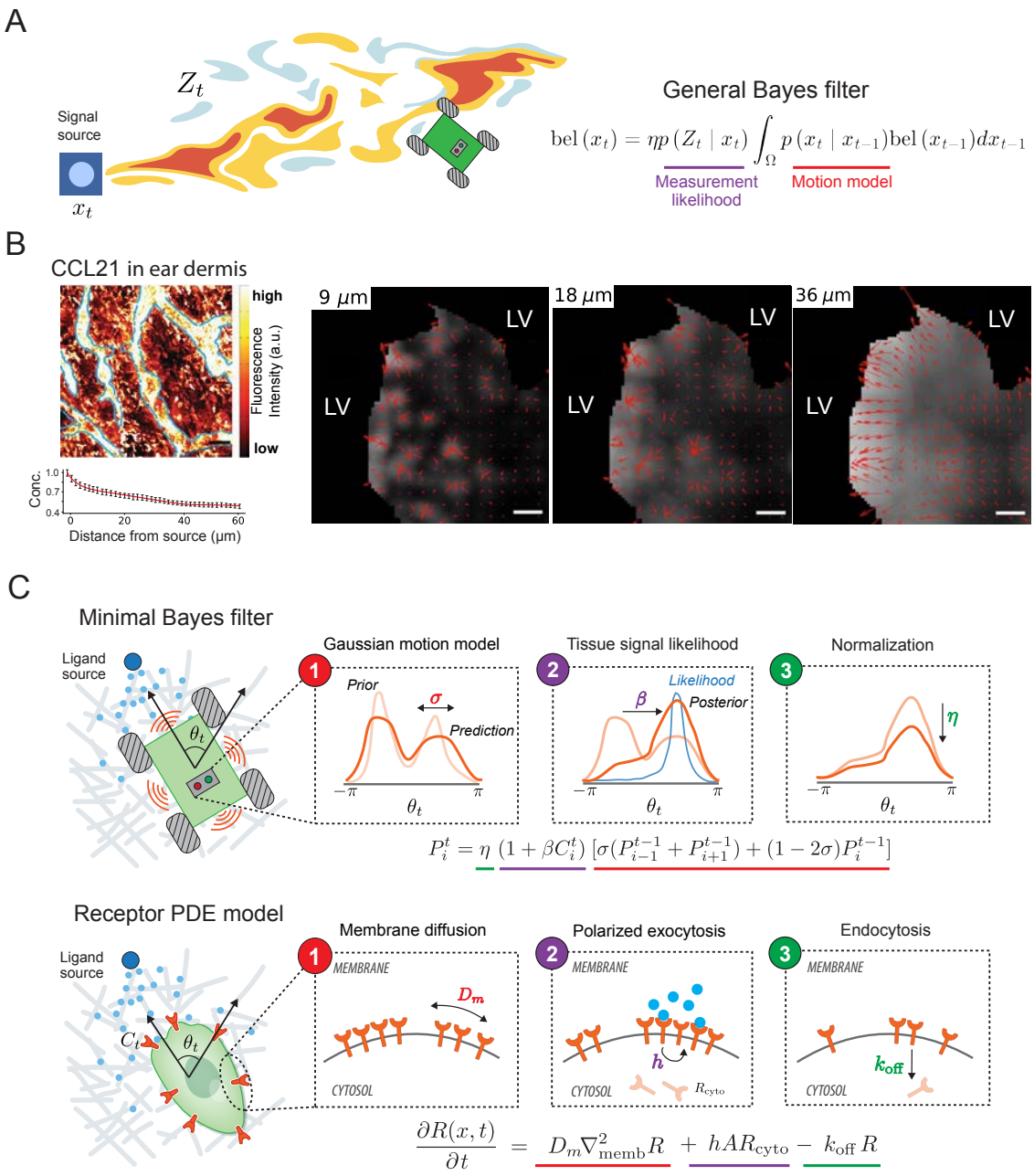

Figure 1: **Mapping receptor dynamics to Bayes filtering.** (**A**) General Bayes filter update equation for source seeking tasks such as plume tracking. (**B**) (Left) ECM-bound CCL21 in mouse ear dermis, and mean signal intensities relative to average maximum signal ± SEM as function of distance from the nearest LV margin. (Right) Red vectors indicate the direction and magnitude of local [CCL21] increase, computed by averaging over a circular surface area corresponding to different virtual cell size. Grayscale indicates the mean CCL21 intensity within each area. Scale bar, 15μm. CCL21 images adapted from (*7*). (**C**) Mathematical equivalence between three steps of a Bayes filter update and three intracellular processes of a receptor PDE model.

In vivo receptor rearrangement matches evolution of Bayes belief distribution

Live-cell imaging and spatial proteomics show that Bayes filtering accurately predicts cell-surface receptor dynamics during source seeking (Figure 2A).

In living cells, the spatial distribution of migratory receptors such as DCC evolves in a manner that mirrors Bayesian belief updates (Figure 2B). In animals, DCC (deleted in colorectal cancer) directs growth cone migration towards its extracellular ligand netrin. Live-cell imaging of the DCC orthologue UNC-40 in *C. elegans* shows that UNC-40 on the surface of anchor cells polarizes toward UNC-6 (netrin) during invasion and continuously redistributes in response to changing extracellular ligand distributions (Figure 2B) (*27*). Notably, when we feed the ligand kymograph as input to the Bayesian filtering algorithm, the evolution of the belief distribution (Equation 4) closely mirrors the observed receptor/F-actin distribution on the cell membrane (Figure 2B). This belief update also matches receptor dynamics simulated by the receptor PDE model (Equation 5), supporting the fact that cells implement Bayesian filtering through receptor rearrangement.

We find a similar pattern of receptor polarization in T cells from intact human tissue. Single-cell spatial proteomic profiling using Imaging Mass Cytometry (IMC) reveals that chemokine receptors, CXCR4, are significantly polarized in CD8+ T cells found in tumor (*28*) (Figure 2C). We quantified receptor polarity as the normalized vector sum of membrane intensity:

$$\text{Polarity} \;=\; \frac{\left\|\sum_i I_i^+ \,\mathbf{u}_i\right\|}{\sum_i I_i^+}$$

where $I_i^+ = \max\left(I_i - \bar{I},\, 0\right)$ is the contrast-enhanced receptor intensity at the i-th membrane pixel, $\bar{I}$ is the mean membrane intensity, and $\mathbf{u}_i$ is the unit vector from the cell centroid to pixel i. For cells localizing to signal source, the Bayes filtering equation predicts that 1) signal receptor distributions should be polarized rather than uniform and 2) cells in similar local environments should exhibit aligned receptor polarity. As predicted, observed CXCR4 polarity in T cells is significantly higher than in randomly shuffled controls (Figure 2D). Furthermore, CXCR4 polarity vectors of nearby T cells ($\leq 50\mu m$) are strongly aligned (p-value: 0.0009), whereas those of distant cells ($\geq 500\mu m$) are randomly oriented (Figure 2E,F). This distance-dependent alignment is specific to the chemokine receptor: other surface proteins such as TIM3 and CD45 show no such pattern (Figure 2G), demonstrating that CXCR4 distributions are actively shaped by ligand distributions in vivo as predicted by the Bayes filtering equation.

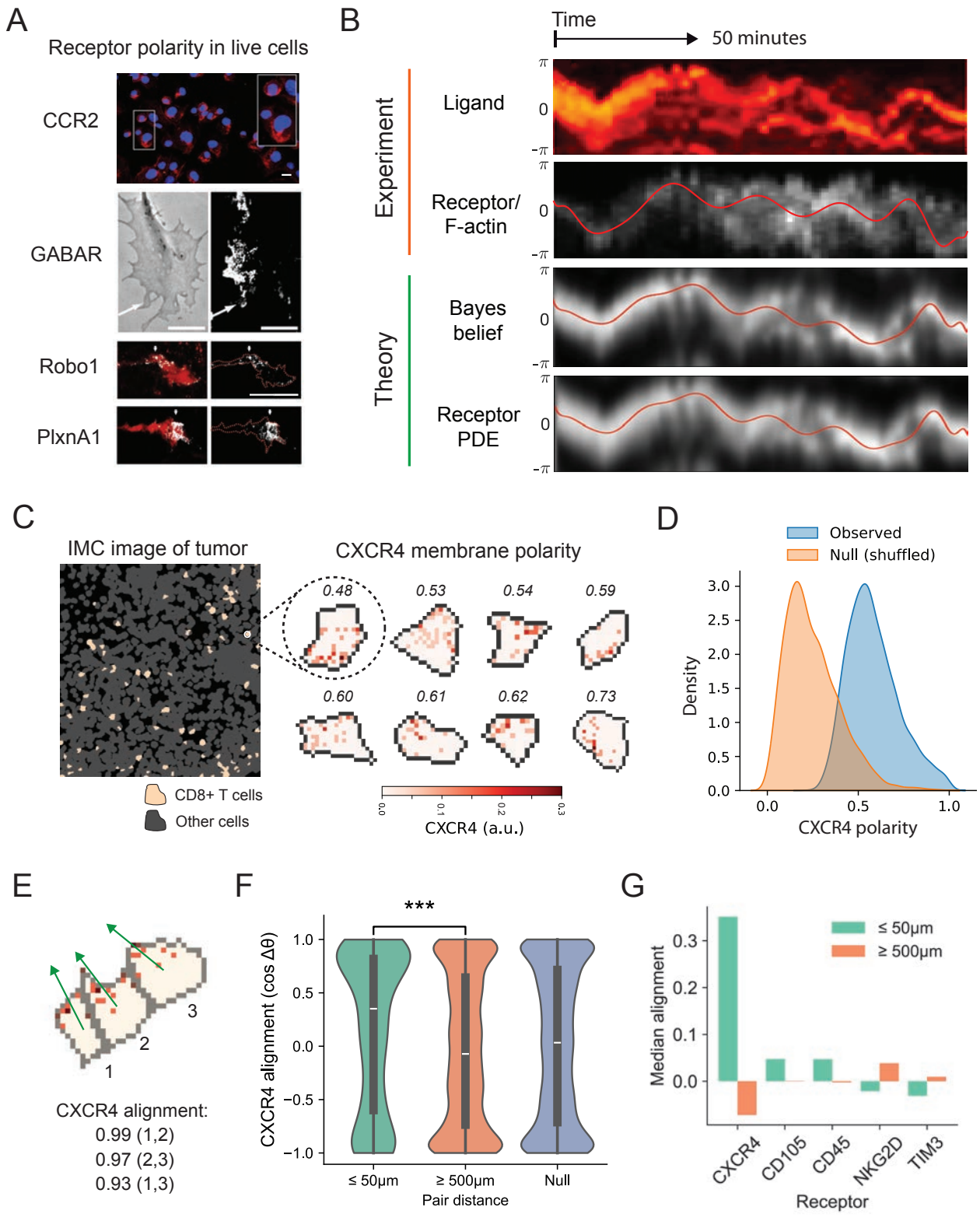

Figure 2: **Bayes filtering update equation predicts in vivo receptor rearrangement.**

Figure 2: (**A**) Live-cell imaging of receptor membrane distribution, white arrow in GABAR image indicates direction of ligand gradient. Scale bar: $10\mu m$. Images adopted from (*14, 15, 18*). (**B**) Kymographs of UNC-6 present around the surface of an anchor cell during invasion, membrane distribution of f-actin in the same cell (highly correlated with UNC-40). Images adopted from (*27*). Belief distribution and receptor PDE output generated using ligand kymograph as input. (**C**) Example IMC image with example cells showing CXCR4 polarization. (**D**) Observed distribution of CXCR4 polarity among T cells in IMC dataset, Null distribution generated by randomly shuffling membrane pixels within individual cells. (**E**) Example of a T cell cluster with strongly aligned CXCR4 polarization found in IMC images. (**F**) Violin plots showing distribution of alignments computed between all pairs of T cells (cosine of difference in polarity angle) within $50\mu m$ or greater than $500\mu m$ apart. Null distribution represents randomly generated vector pairs. (**G**) Median alignment for different receptors.

Receptor redistribution overcomes patchy gradients

Simulations show that Bayes filtering and its biophysical implementation via receptor redistribution enable robust navigation in patchy interstitial gradients.

To model these challenging environments (*16*), we simulate fluid flow carrying signaling ligands through an irregular ECM network, generating realistic patchy ligand distributions (Figure 3A). These simulated patterns closely resemble experimentally observed chemokine gradients (Figure 1B). In both tissue imaging and simulation, local gradient directions experienced by a typical cell (10-20 μm in diameter) fail to align with the global gradient direction, whereas larger cells (40μm) do not experience this misalignment (Figure 3B).

Cells simulated with receptor redistribution rapidly localize to the ligand source in patchy gradients, effectively avoiding signal traps (Figure 3B). We evaluate navigation efficiency by comparing simulations of four strategies: gradient tracking, receptor redistribution, bayes filtering, and Local Excitation-Global Inhibition (LEGI) (*16*). Gradient-tracking cells strictly follow the direction of local ligand gradient and become trapped in local peaks (Figure 3B), failing to cross the 60 μm gradient even after three hours. LEGI, which selectively amplifies spatial signals to track shallow gradients (*29*), also fails under these conditions. In contrast, receptor redistribution (and Bayes

filtering) enable cells to consistently reach the source (Figure 3C), overcoming local traps by following the direction of maximal receptor activity (or belief) at each step, either through the bayesian update rule (Equation 4) or its implementation via receptor dynamics (Equation 5). All simulations used physiologically plausible parameters (*16*).

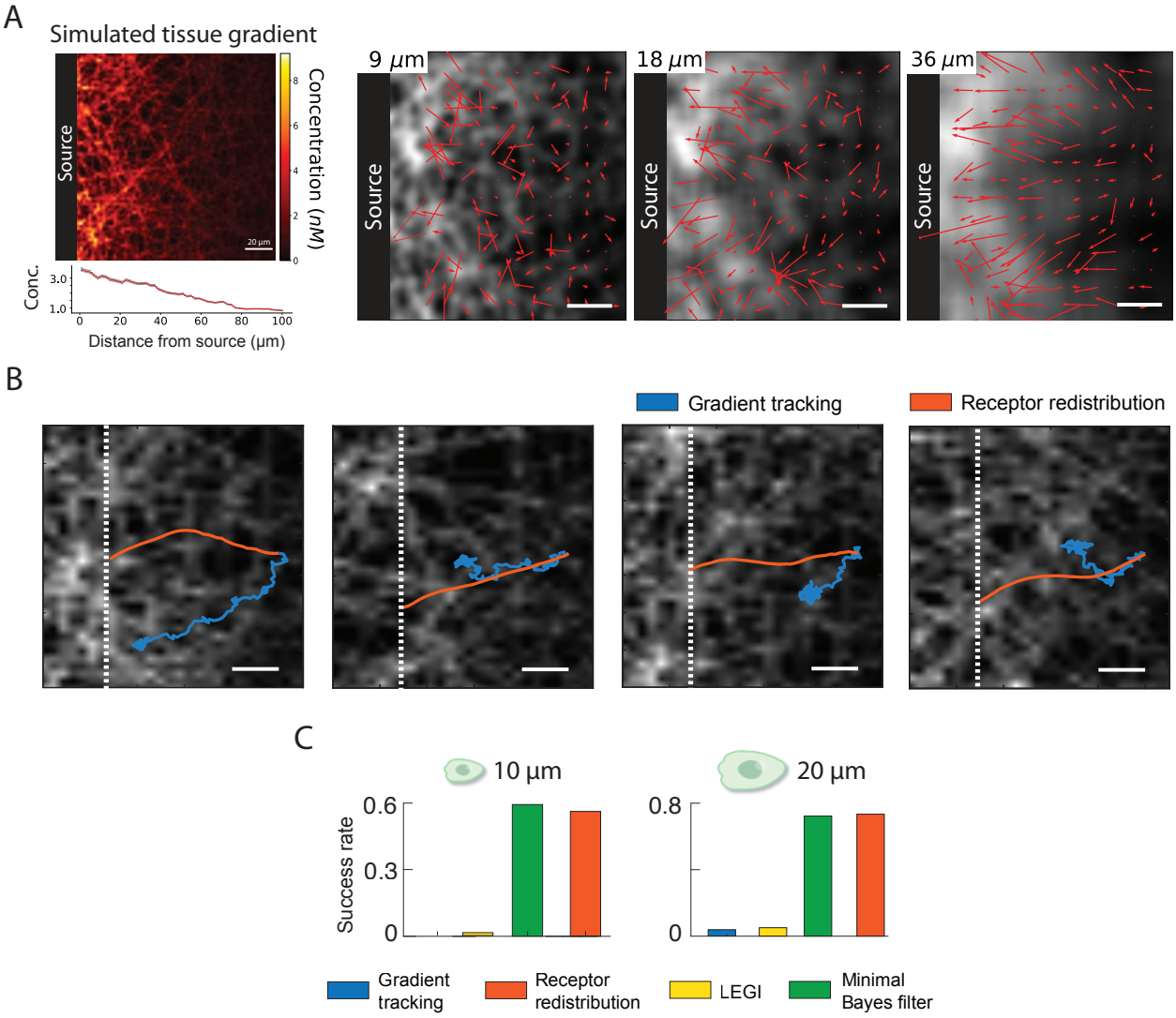

Figure 3: **Comparing navigation strategies in patchy gradient.** (**A**) Simulated ECM-bound gradient (right). Vector maps of local gradients as observed by virtual cells of a given diameter; Scale bar, $15\mu m$. (**B**) Simulated trajectories for cells following local gradient vs. using receptor redistribution; Signal source is at the left boundary. (**C**) Navigation success rate for cells using naive gradient tracking, receptor redistribution (Equation 5), Local Excitation Global Inhibition (LEGI), and minimal Bayes filter (Equation 4).

Cellular implementation extends beyond standard Bayes filtering

A distinctive feature of cellular Bayes filtering (Equation 5), distinct from standard robotics implementations (Equation 1), is the coupling between observed signals and the motion model (Figure 4A). When mapping Bayesian filtering to receptor redistribution (Figure 1C), we found that membrane diffusivity of receptors corresponds to the variance of the motion model. In cells, receptor activation via ligand binding reduces receptor diffusivity through multiple mechanisms (Figure 4A), effectively lowering the variance parameter of the motion model as signal strength increases. This coupling extends the cell's implementation from a standard filter to an adaptive one.

This signal-variance coupling improves source-seeking performance in environments with fluctuating noise. In robot simulations (Figure 4B), a standard Extended Kalman filtering (EKF) maintains a fixed motion model variance equal to the true motion variance,

$$\sigma^2_{\text{standard}} = \sigma^2_{\text{true}},$$

whereas our "cell-inspired EKF" adjusts variance according to the observed signal Z_t,

$$\sigma^2_{\text{cell-inspired}} = \frac{\sigma^2_{\text{true}}}{1 + Z_t}. \tag{6}$$

Incorporating this coupling reduced mean time-to-target 2–4 folds across a wide range of noise levels (Figure 4C, D).

We can understand the benefit of this receptorÐsignal coupling in terms of filter gain, which quantifies the degree to which new observations influence the belief (posterior) about the systemÕs state. For Poisson-distributed signals, stronger signal implies larger variability. In regimes of strong signal, therefore, cells and robots reduce their reliance on instantaneous observations by lowering the filter gain – precisely the effect achieved by decreasing motion model variance (*16*). It follows that an Adaptive EKF, which must continuously adjust the covariance term in the measurement likelihood to track changing noise statistics, achieves optimal performance. Remarkably, the cell-inspired EKF achieves nearly identical performance without the additional computation required to estimate measurement covariance (Figure 4D).

In conclusion, coupling receptor diffusivity to ligand engagement extends cellular Bayes filtering from a standard to an adaptive filter, enabling robust inference under fluctuating noise without the need for explicit noise estimation.

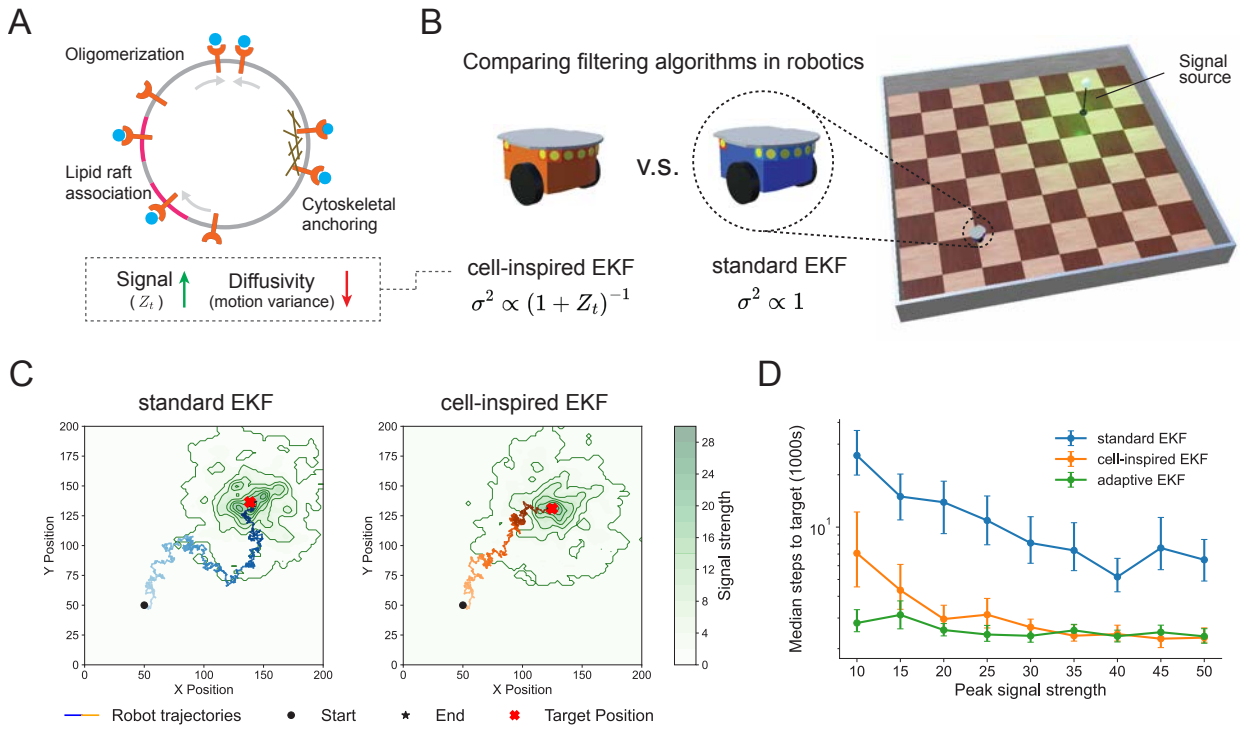

Figure 4: **Cell-inspired, signal-coupled motion model for robotic navigation.** (**A**) Multiple cellular mechanisms couple receptor activity (signal) with receptor diffusivity (motion model variance). (**B**) Image of simulated arena with robot and signal source. (**C**) Simulated trajectories of robots solving a target navigation task (*16*) using either standard Extended Kalman Filtering or coupled EKF which includes a signal-coupled motion model (Equation 6). (**D**) Navigation efficiency of three versions of EKF across environments with different peak signal strength; error bar represents SEM.

Bayesian formalism predicts cell constraints

The mapping between the Bayesian formulation and the receptor PDE model predicts a coupling between cell speed and receptor dynamics.

In standard robotic implementations of Bayes filtering, the variance parameter σ of the motion model typically increases with robot speed (Equation 2). This relationship arises because faster motion accumulates greater positional uncertainty, as even small directional errors translate into larger spatial deviations over longer trajectories. Given that our mapping connects the motion model's variance parameter σ to the receptor diffusivity D_m (Figure 1C), we predict that optimal receptor diffusivity should scale with cell speed. Indeed, our simulations confirm this prediction (Figure 5A), demonstrating that higher cell speeds require greater receptor diffusivity (Figure 5B). Intuitively, a fast-moving cell encounters new environmental signals more frequently and must thus rapidly revise its priors. Faster receptor diffusivity enables these rapid updates. Note Figure 5A also suggests that a fixed, low receptor diffusivity can still support efficient migration, despite being suboptimal.

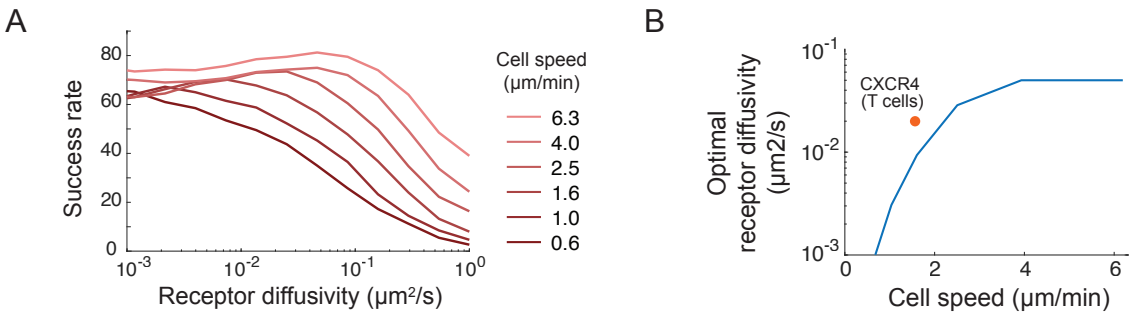

Figure 5: **Bayesian formalism predicts optimal receptor diffusivity.** (**A**) Success rate for cells simulated with different migration speed and receptor diffusivity. (**B**) Optimal receptor diffusivity at various cell speed, dot showing empirical data for CXCR4 in Jurkat T cells (*30, 31*).

Discussion

In this work, we investigated the problem of source seeking by cells in complex tissue environments and established a direct mapping between receptor dynamics and Bayesian filtering, a widely used algorithm in robotic source seeking. This mapping shows that receptor redistribution can enable cells to efficiently navigate interstitial gradients, overcoming localized signal patches. This mapping also reveals a unique feature of the cellular Bayesian filter not present in standard Bayes filtering: the coupling between the observed signal and the motion model, which effectively acts as an adaptive Bayes filter enabling cells to adapt to fluctuating noise statistics.

Alternative implementations of Bayesian filtering in cells need not require receptor redistribution. The evolving belief distribution can instead be stored in the spatial distribution of signaling molecules that are recruited to the inner leaflet of the plasma membrane when receptors become active. In this scheme, the observed signal, C, driving the filter are receptor activation events, not extracellular ligand counts. After activation, many receptors (e.g., GPCRs) recruit cytosolic effectors, such as heterotrimeric G-proteins, adaptors, lipid kinases, to the membrane. Positive feedback loops (e.g. PI3K-Rac-F-action (*32*)) amplify and stabilize these effectors, effectively integrating the spatial distribution of recent receptor activity into the distribution of membrane-bound effectors. Because most membrane-bound effectors diffuse laterally, these molecules also naturally perform the prediction step involving the motion model, propagating the belief without requiring receptor relocation. Our Bayesian framework therefore applies to any membrane-associated species that (i) is produced or recruited in proportion to receptor activity and (ii) diffuses laterally, expanding the biochemical strategies cells might use to integrate noisy environmental cues.

Our work opens up new experimental directions. Future studies can leverage protein micropatterning to construct in vitro mimics of complex ligand landscapes observed in tissue, enabling simultaneous visualization of ligand distribution and the dynamics of surface receptors in migrating cells. These tools can be used to investigate how receptors in different cell types with different redistribution mechanisms (e.g., actin- vs. microtubule-based transport) differ in their responses to spatial signal structure.

Our work connects to a broader framework proposed by neuroscientist David Marr. Marr proposed that understanding an information-processing system requires analyzing it at three levels (*33*):

the computational problem it solves, the algorithm it uses, and the physical implementation of that algorithm. This framework guides our analysis: starting from a navigation problem, we identify a Bayesian algorithm that solves it, and then show how mechanisms of receptor redistribution, as observed in cells, can implement this algorithm. Additional algorithmic strategies for decision making in complex environments may emerge from careful analysis of biological systems.

References and Notes

1. A. Francis, S. Li, C. Griffiths, J. Sienz, Gas source localization and mapping with mobile robots: A review. *Journal of Field Robotics* **39** (8), 1341–1373 (2022).

2. W. Naeem, R. Sutton, J. Chudley, Chemical plume tracing and odour source localisation by autonomous vehicles. *The Journal of Navigation* **60** (2), 173–190 (2007).

3. S. Thrun, W. Burgard, D. Fox, *Probabilistic robotics* (MIT Press, Cambridge, Mass.) (2005).

4. D. J. Fowell, M. Kim, The spatio-temporal control of effector T cell migration. *Nature Reviews Immunology* pp. 1–15 (2021).

5. E. Russo, *et al.*, Intralymphatic CCL21 promotes tissue egress of dendritic cells through afferent lymphatic vessels. *Cell reports* **14** (7), 1723–1734 (2016).

6. A. C. von Philipsborn, *et al.*, Growth cone navigation in substrate-bound ephrin gradients. *Development* **133** (13), 2487–2495 (2006).

7. M. Weber, *et al.*, Interstitial dendritic cell guidance by haptotactic chemokine gradients. *Science* **339** (6117), 328–332 (2013).

8. Z. J. Wang, M. Thomson, Localization of signaling receptors maximizes cellular information acquisition in spatially structured natural environments. *Cell Systems* **13** (7), 530–546 (2022).

9. T. E. Sutherland, D. P. Dyer, J. E. Allen, The extracellular matrix and the immune system: A mutually dependent relationship. *Science* **379** (6633), eabp8964 (2023).

10. T. E. Kennedy, H. Wang, W. Marshall, M. Tessier-Lavigne, Axon guidance by diffusible chemoattractants: a gradient of netrin protein in the developing spinal cord. *Journal of Neuroscience* **26** (34), 8866–8874 (2006).

11. M. Sarris, *et al.*, Inflammatory chemokines direct and restrict leukocyte migration within live tissues as glycan-bound gradients. *Current Biology* **22** (24), 2375–2382 (2012).

12. E. Donà, *et al.*, Directional tissue migration through a self-generated chemokine gradient. *Nature* **503** (7475), 285–289 (2013).

13. C. Guirland, S. Suzuki, M. Kojima, B. Lu, J. Q. Zheng, Lipid rafts mediate chemotropic guidance of nerve growth cones. *Neuron* **42** (1), 51–62 (2004).

14. A. Pignata, *et al.*, A spatiotemporal sequence of sensitization to slits and semaphorins orchestrates commissural axon navigation. *Cell reports* **29** (2), 347–362 (2019).

15. F. Belema-Bedada, S. Uchida, A. Martire, S. Kostin, T. Braun, Efficient homing of multipotent adult mesenchymal stem cells depends on FROUNT-mediated clustering of CCR2. *Cell stem cell* **2** (6), 566–575 (2008).

16. Materials and methods are available as supplementary material.

17. C. C. Winkle, *et al.*, A novel Netrin-1–sensitive mechanism promotes local SNARE-mediated exocytosis during axon branching. *Journal of Cell Biology* **205** (2), 217–232 (2014).

18. C. Bouzigues, M. Morel, A. Triller, M. Dahan, Asymmetric redistribution of GABA receptors during GABA gradient sensing by nerve growth cones analyzed by single quantum dot imaging. *Proceedings of the National Academy of Sciences* **104** (27), 11251–11256 (2007).

19. A. W. McClure, *et al.*, Role of polarized G protein signaling in tracking pheromone gradients. *Developmental cell* **35** (4), 471–482 (2015).

20. M. Shimonaka, *et al.*, Rap1 translates chemokine signals to integrin activation, cell polarization, and motility across vascular endothelium under flow. *The Journal of cell biology* **161** (2), 417–427 (2003).

21. T. Tojima, *et al.*, Attractive axon guidance involves asymmetric membrane transport and exocytosis in the growth cone. *Nature neuroscience* **10** (1), 58–66 (2007).

22. P. Wan, *et al.*, Guidance receptor promotes the asymmetric distribution of exocyst and recycling endosome during collective cell migration. *Development* **140** (23), 4797–4806 (2013).

23. J. Zeng, S. Feng, B. Wu, W. Guo, Polarized exocytosis. *Cold Spring Harbor perspectives in biology* **9** (12), a027870 (2017).

24. T. Cotrufo, *et al.*, A signaling mechanism coupling netrin-1/deleted in colorectal cancer chemoattraction to SNARE-mediated exocytosis in axonal growth cones. *Journal of Neuroscience* **31** (41), 14463–14480 (2011).

25. G. Servant, O. D. Weiner, E. R. Neptune, J. W. Sedat, H. R. Bourne, Dynamics of a chemoattractant receptor in living neutrophils during chemotaxis. *Molecular biology of the cell* **10** (4), 1163–1178 (1999).

26. G. Servant, *et al.*, Polarization of chemoattractant receptor signaling during neutrophil chemotaxis. *Science* **287** (5455), 1037–1040 (2000).

27. Z. Wang, *et al.*, UNC-6 (netrin) stabilizes oscillatory clustering of the UNC-40 (DCC) receptor to orient polarity. *Journal of Cell Biology* **206** (5), 619–633 (2014).

28. Z. Wang, *et al.*, Extracellular vesicles in fatty liver promote a metastatic tumor microenvironment. *Cell metabolism* **35** (7), 1209–1226 (2023).

29. Y. Xiong, C.-H. Huang, P. A. Iglesias, P. N. Devreotes, Cells navigate with a local-excitation, global-inhibition-biased excitable network. *Proceedings of the National Academy of Sciences* **107** (40), 17079–17086 (2010).

30. X. Yin, D. A. Knecht, M. A. Lynes, Metallothionein mediates leukocyte chemotaxis. *BMC immunology* **6** (1), 21 (2005).

31. E. M. García-Cuesta, *et al.*, Allosteric modulation of the CXCR4: CXCL12 axis by targeting receptor nanoclustering via the TMV-TMVI domain. *Elife* **13**, RP93968 (2024).

32. T. Inoue, T. Meyer, Synthetic activation of endogenous PI3K and Rac identifies an AND-gate switch for cell polarization and migration. *PloS one* **3** (8), e3068 (2008).

33. D. Marr, T. Poggio, *From Understanding Computation to Understanding Neural Circuitry*, Tech. rep., USA (1976).

34. K. A. Rejniak, *et al.*, The role of tumor tissue architecture in treatment penetration and efficacy: an integrative study. *Frontiers in oncology* **3**, 111 (2013).

35. F. Milde, M. Bergdorf, P. Koumoutsakos, A hybrid model for three-dimensional simulations of sprouting angiogenesis. *Biophysical journal* **95** (7), 3146–3160 (2008).

36. X. Wang, M. R. Lennartz, D. J. Loegering, J. A. Stenken, Multiplexed cytokine detection of interstitial fluid collected from polymeric hollow tube implantsâĂŤa feasibility study. *Cytokine* **43** (1), 15–19 (2008).

37. K. E. Clark, *et al.*, Multiplex cytokine analysis of dermal interstitial blister fluid defines local disease mechanisms in systemic sclerosis. *Arthritis research & therapy* **17** (1), 1–11 (2015).

38. D. Harjanto, M. H. Zaman, Modeling extracellular matrix reorganization in 3D environments. *PLoS One* **8** (1), e52509 (2013).

39. D. K. Schlüter, I. Ramis-Conde, M. A. Chaplain, Computational modeling of single-cell migration: the leading role of extracellular matrix fibers. *Biophysical journal* **103** (6), 1141–1151 (2012).

40. B. Lee, *et al.*, A three-dimensional computational model of collagen network mechanics. *PloS one* **9** (11), e111896 (2014).

41. P. Friedl, *et al.*, Migration of highly aggressive MV3 melanoma cells in 3-dimensional collagen lattices results in local matrix reorganization and shedding of $\alpha 2$ and $\beta 1$ integrins and CD44. *Cancer research* **57** (10), 2061–2070 (1997).

42. M. Ueda, Y. Sako, T. Tanaka, P. Devreotes, T. Yanagida, Single-molecule analysis of chemotactic signaling in Dictyostelium cells. *Science* **294** (5543), 864–867 (2001).

43. E. Marco, R. Wedlich-Soldner, R. Li, S. J. Altschuler, L. F. Wu, Endocytosis optimizes the dynamic localization of membrane proteins that regulate cortical polarity. *Cell* **129** (2), 411–422 (2007).

44. B. Hegemann, *et al.*, A cellular system for spatial signal decoding in chemical gradients. *Developmental cell* **35** (4), 458–470 (2015).

45. L. D. L. JJ, Receptors: Models for binding, trafficking, and signaling (1993).

46. S. Pippig, S. Andexinger, M. J. Lohse, Sequestration and recycling of beta 2-adrenergic receptors permit receptor resensitization. *Molecular pharmacology* **47** (4), 666–676 (1995).

47. J. A. Koenig, J. M. Edwardson, Intracellular trafficking of the muscarinic acetylcholine receptor: importance of subtype and cell type. *Molecular pharmacology* **49** (2), 351–359 (1996).

48. J. A. Koenig, J. M. Edwardson, Kinetic analysis of the trafficking of muscarinic acetylcholine receptors between the plasma membrane and intracellular compartments. *Journal of Biological Chemistry* **269** (25), 17174–17182 (1994).

49. C. Shi, C.-H. Huang, P. N. Devreotes, P. A. Iglesias, Interaction of motility, directional sensing, and polarity modules recreates the behaviors of chemotaxing cells. *PLoS computational biology* **9** (7), e1003122 (2013).

50. MATLAB, *23.2.0.2409890 (R2023b)* (The MathWorks Inc., Natick, Massachusetts) (2023).

51. Y. Wang, D. J. Irvine, Convolution of chemoattractant secretion rate, source density, and receptor desensitization direct diverse migration patterns in leukocytes. *Integrative Biology* **5** (3), 481–494 (2013).

52. J. D. Shields, *et al.*, Autologous chemotaxis as a mechanism of tumor cell homing to lymphatics via interstitial flow and autocrine CCR7 signaling. *Cancer cell* **11** (6), 526–538 (2007).

53. L. Martínez-Muñoz, *et al.*, Separating actin-dependent chemokine receptor nanoclustering from dimerization indicates a role for clustering in CXCR4 signaling and function. *Molecular cell* **70** (1), 106–119 (2018).